

Non-Born-Oppenheimer confined variational calculation of low-energy Ps-H₂ scatteringW. Du,^{1,2} M.-S. Wu,^{3,4,*} J.-Y. Zhang^{①,1,†} Y. Qian^{②,5} K. Varga,⁶ and Z.-C. Yan^{7,1}¹*State Key Laboratory of Magnetic Resonance and Atomic and Molecular Physics, Innovation Academy for Precision Measurement Science and Technology, Chinese Academy of Sciences, Wuhan 430071, China*²*School of Physical Sciences, University of Chinese Academy of Sciences, Beijing 100049, China*³*School of Science, Hainan University, Haikou 570228, China*⁴*Center for Theoretical Physics, Hainan University, Haikou 570228, China*⁵*Department of Computer Science and Technology, East China Normal University, Shanghai 200062, China*⁶*Department of Physics and Astronomy, Vanderbilt University, Nashville, Tennessee 37235, USA*⁷*Department of Physics, University of New Brunswick, Fredericton, New Brunswick, Canada E3B 5A3*

(Received 1 March 2022; accepted 28 April 2022; published 20 May 2022)

Using the confined variational method, the low-energy S -wave elastic scattering of positronium from molecular hydrogen is studied nonadiabatically at incident energy up to 0.13 eV. Accurate S -wave phase shifts, scattering lengths, and cross sections are calculated and compared with other theoretical and experimental values. Using the modified effective-range formula, the S -wave scattering length is determined to be 1.97 Bohr radii, which is about 2.5% smaller than that of the confined variational calculation under the fixed-nucleus approximation. The consistency of the present cross sections with those from the angular correlation of annihilation radiation experiment indicates that the results of Doppler broadening spectroscopy might be problematic. We also discuss the distortion effects of positronium and molecular hydrogen.

DOI: [10.1103/PhysRevA.105.052809](https://doi.org/10.1103/PhysRevA.105.052809)**I. INTRODUCTION**

Positronium (Ps) is a metastable bound system consisting of an electron and a positron with a ground-state lifetime of 0.125 ns for the spin-singlet state (p -Ps) and 142 ns for the spin-triplet state (o -Ps). As a purely leptonic system, Ps is an ideal testing ground for quantum electrodynamics [1–5], such as the “Ps fine-structure puzzle” [5]. Furthermore, with the advancement of Ps beam techniques [6–10], Ps-antiproton [11,12], Ps-atom, and Ps-molecule collisions have attracted considerable attention both experimentally and theoretically [9,11–21]. Interestingly, an electron and Ps have similar total scattering cross sections for the same incident velocity when scattering by He, Ar, Kr, Xe, H₂, N₂, O₂, and SF₆ at intermediate energies [14] due to the diffusion of Ps and the stronger interaction of the electron than positron with targets in this energy region [22].

Ps-H₂ scattering is of particular interest because H₂ is the simplest molecule and thus can be considered a benchmark system for studying Ps-molecule scattering. Experimentally, Nagashima *et al.* [23] measured the momentum-transfer cross section at a Ps average energy of 0.046 eV using the angular correlation of the annihilation radiation method. Saito *et al.* [24] obtained a momentum-transfer cross section below 0.3 eV using the same method. Using the Doppler broadening spectroscopy, Skalsey *et al.* [25,26] measured the momentum-transfer cross section at scattering energy ranging from 0.39 to 3.0 eV. Although these experiments can achieve lower

scattering energies, the accuracy of the measurements is low. A significant advance was made by Garner *et al.* [6–8] using a Ps beam, in which they directly measured the total cross sections for the scattering energy from 10 to 120 eV. With further improvement of Ps beam quality, total cross sections with incident energy from 6.8 to 109 eV were obtained by Brawley *et al.* [14], and similarities between Ps and electrons in the shape and magnitude of the total cross sections at the same incident velocity were observed. However, cross sections with Ps beam energy below the Ps excitation threshold (5.1 eV) are rarely measured.

There are many theoretical studies on Ps-H₂ scattering using various approaches, including the perturbative calculation by Comi *et al.* [27], the first Born approximation by Biswas and Ghosh [28], the coupled-channel calculation by Biswas and Adhikari [29,30], the pseudopotential method and the binary-encounter approximation by Wilde and Fabrikant [21], the confined variational method (CVM) by Zhang *et al.* [31], and the free-electron-gas approximation plus an orthogonalizing pseudopotential by Wilde and Fabrikant [32]. The complicated Coulomb correlations between scattering particles and the electron exchange in Ps-H₂ have been only partially considered except for the calculations of Zhang *et al.* [31]. However, all the previous works were carried out in the framework of the Born-Oppenheimer approximation.

The confined variational method, an *ab initio* approach for studying low-energy elastic-scattering problems, has been used extensively [31,33–36]. Recently, we developed a strategy that can effectively eliminate nonphysical confinement effects of the original CVM [37,38]. In addition, contrary to the original CVM, the strategy of using a smaller constraint radius R_0 can greatly reduce the computational cost [37,38].

*mswu@hainanu.edu.cn

†jzhang@apm.ac.cn

The purpose of this paper is to present our study of low-energy S -wave elastic Ps-H₂ scattering using CVM by treating Ps-H₂ as a six-body Coulomb system without the Born-Oppenheimer approximation (non-BO). This paper is organized as follows. In Sec. II, the CVM is introduced. The computational results are presented in Sec. III, which includes the S -wave phase shifts in Sec. III A, the S -wave scattering lengths and cross sections in Sec. III B, and the distortion effects in Sec. III C. Finally, we give a summary in Sec. IV. Atomic units are used throughout unless otherwise stated.

II. THEORY

For the Ps-H₂ scattering, the Hamiltonian operator in the laboratory frame can be expressed as

$$\mathcal{H} = \sum_{i=0}^5 \frac{\mathbf{p}_i^2}{2m_i} + \sum_{\substack{i,j=0 \\ j>i}}^5 \frac{q_i q_j}{|\mathbf{r}_i - \mathbf{r}_j|}, \quad (1)$$

where \mathbf{r}_i , m_i , and q_i represent, respectively, the position vector, mass, and charge of the i th particle and \mathbf{p}_i is the momentum conjugate to \mathbf{r}_i . The two protons are labeled particles 0 and 1; the three electrons are labeled 2, 3, and 4, and the positron is labeled 5. Furthermore, if we choose the zeroth particle as the reference particle, after eliminating the center-of-mass motion, the internal Hamiltonian has the following form:

$$H = \frac{1}{2} \sum_{i,j=1}^5 \Lambda_{ij} \pi_i \cdot \pi_j + \sum_{i=1}^5 \frac{q_0 q_i}{|\mathbf{x}_i|} + \sum_{\substack{i,j=1 \\ j>i}}^5 \frac{q_i q_j}{|\mathbf{x}_i - \mathbf{x}_j|}, \quad (2)$$

where $\mathbf{x}_i = \mathbf{r}_i - \mathbf{r}_0$, $\pi_i = -i\partial/\partial\mathbf{x}_i$, and $\Lambda_{ij} = \sum_{k=1}^6 U_{ik} U_{jk} / m_k$, with U being the transformation matrix

$$U = \begin{pmatrix} -1 & 1 & 0 & \cdots & 0 \\ -1 & 0 & 1 & \cdots & 0 \\ \vdots & & & & \vdots \\ -1 & 0 & 0 & \cdots & 1 \\ \frac{m_0}{m_i} & \frac{m_1}{m_i} & \frac{m_2}{m_i} & \cdots & \frac{m_5}{m_i} \end{pmatrix}. \quad (3)$$

In the above equation, $m_t = \sum_{i=0}^5 m_i$ is the total mass of the system.

After adding a confining potential V_{cp} in the Hamiltonian H , the CVM converts the original many-body scattering problem into a confined many-body bound-state one,

$$(H + V_{\text{cp}})\Psi(\mathbf{x}, \mathbf{s}) = E\Psi(\mathbf{x}, \mathbf{s}), \quad (4)$$

where \mathbf{x} denotes, collectively, $(\mathbf{x}_1, \mathbf{x}_2, \mathbf{x}_3, \mathbf{x}_4, \mathbf{x}_5)$; \mathbf{s} denotes $(\mathbf{s}_0, \mathbf{s}_1, \mathbf{s}_2, \mathbf{s}_3, \mathbf{s}_4, \mathbf{s}_5)$ of the six particle spins; and Ψ is the eigenfunction of $H + V_{\text{cp}}$ corresponding to E . It is understood that E is the total energy of the original scattering system, which includes the ground-state energies of Ps and H₂ and the scattering energy E_s , i.e., $E = E_{\text{Ps}} + E_{\text{H}_2} + E_s$. The relation between the scattering energy E_s and the scattering momentum k is $E_s = k^2/(2\mu)$, where $\mu = 1.998\,911\,951$ is the reduced mass between Ps and H₂. To describe the complicated Coulomb correlations between particles, the many-body wave function Ψ is expanded in terms of explicitly correlated

Gaussian (ECG) functions [39],

$$\Psi = \sum_{n,i} C_n \hat{P}_i \phi_n, \quad (5)$$

$$\phi_n = \frac{1}{\sqrt{4\pi}} |\mathbf{x}_1|^{2K} \exp\left(-\frac{1}{2} \mathbf{x}^T A_n \mathbf{x}\right) \chi(\mathbf{s}),$$

$$\chi(\mathbf{s}) = (\alpha_0 \beta_1 - \beta_0 \alpha_1)(\alpha_2 \beta_3 - \beta_2 \alpha_3) \alpha_4 \alpha_5,$$

where $\{C_n\}$ are the linear coefficients determined by solving the generalized eigenvalue problem (4), $\{\hat{P}_i\}$ are permutation operators of identical particles, $\chi(\mathbf{s})$ is the chosen spin function, A_n is a symmetric positive-definite matrix of real parameters, K is a positive integer, and $|\mathbf{x}_1|^{2K}$ is an important factor to describe the relative motion between the two protons. Due to the fact that the Hamiltonian operator \mathcal{H} is independent of particle spins, our results are suitable for the scattering of both parapositronium and orthopositronium.

The confining potential used in this work [33] has the form

$$V_{\text{cp}} = \sum_{i=2}^4 v_{\text{cp}}(\rho_i), \quad (6)$$

where

$$v_{\text{cp}}(\rho_i) = \begin{cases} 0, & \rho_i < R_0, \\ G(\rho_i - R_0)^2, & \rho_i \geq R_0, \end{cases} \quad (7)$$

and ρ_i is the distance between the center of mass of H₂ and the center of mass of Ps composed of the i th electron and the positron. The confining radius R_0 should be large enough to ensure that the complicated short-range interaction between Ps and H₂ can be ignored outside the sphere of radius R_0 . To eliminate unphysical confining effects, we define the following judgment index s_i^{nm} between two basis functions ϕ_n and ϕ_m :

$$s_i^{nm} = \frac{\langle \phi_n | \Theta(x_{i5} - R_1)(x_{i5} - R_1)^2 | \phi_m \rangle}{\langle \phi_n | \Theta(\rho_i - R_0)(\rho_i - R_0)^2 | \phi_m \rangle}, \quad (8)$$

where $x_{i5} = |\mathbf{x}_i - \mathbf{x}_5|$, with $2 \leq i \leq 4$, Θ is the Heaviside step function, and R_1 is an adjustable parameter. In this work, we discard $\langle \phi_n | v_{\text{cp}}(\rho_i) | \phi_m \rangle$ when s_i^{nm} is larger than 1.0 [37,38].

The confining potential parameter G in Eq. (7) is tuned to ensure that a specific total energy E (or the scattering momentum k) is yielded. The variational process of solving the eigenenergies of the confined Ps-H₂ system is the most time-consuming part of our calculation. The stochastic variational method is applied to optimize the nonlinear parameter matrices $\{A_n\}$. Once the confining potential $v_{\text{cp}}(\rho)$ is determined, we then use the associated Laguerre polynomials $L_n^{\alpha}(\rho)$ as basis functions and solve the one-dimensional bound-state problem

$$\left(-\frac{1}{2\mu} \nabla^2 + V_m(\rho) + v_{\text{cp}}(\rho)\right) \Phi(\rho) = E' \Phi(\rho), \quad (9)$$

where the model potential V_m is determined to produce the same scattering energy, i.e., $E' = E_s$, under the same confining potential v_{cp} . The convergence of this step is checked by using different sizes of basis set, different α_b , and different grids of numerical integration. The main requirement for V_m is that its short-range part vanishes at R_0 . We choose $V_m(\rho)$ to

be

$$V_m(\rho) = \lambda e^{-\alpha\rho} - \frac{C_6}{\rho^6}(1 - e^{-(\rho/\beta)^6}), \quad (10)$$

where λ , α , and β are adjustable parameters and $C_6 = 49.3$ is the van der Waals coefficient [20]. The second term in Eq. (10) is to correctly describe the interaction between Ps and H₂ in the asymptotic region, the region outside the sphere of radius R_0 . We fix $\alpha = 0.5$ and $\beta = 5$ and adjust only λ so that the eigenvalue of Eq. (9) is $E' = k^2/(2\mu)$ for given k . Subsequently, we solve the only scattering equation for V_m ,

$$\left(-\frac{1}{2\mu}\nabla^2 + V_m(\rho)\right)\Phi'(\rho) = E'\Phi'(\rho). \quad (11)$$

After choosing $\Phi'(\rho) = \varphi(\rho)/(k\rho)$ for the S -wave scattering, we have $\{\frac{d^2}{d\rho^2} + 2\mu[E' - V_m(\rho)]\}\varphi(\rho) = 0$. The asymptotic form of $\varphi(\rho)$ is $A\sin(k\rho + \delta_k)$, with A being an unknown constant. Then the logarithmic derivative $\Gamma(\rho)$ of $\varphi(\rho)$ is propagated to $\rho = 500$ using Johnson's log-derivative method. Then the phase shift δ_k is obtained by comparing the numerical value of $\Gamma(\rho = 500)$ to the corresponding asymptotic form $k\cot(500k + \delta_k)$. The convergence of this step is checked with different maximum values of ρ and different grids of the numerical integration. The key point of the CVM is that the logarithmic derivatives of the wave functions Ψ , Φ , and Φ' are exactly the same as that of the original scattering wave function for the same energy E_s at R_0 . In addition, the phase shift is a function of the logarithmic derivative. Therefore, the phase shift obtained from solving the $V_m(\rho)$ scattering problem is equal to that of the Ps-H₂ elastic scattering. For more details about the CVM, the reader is referred to Refs. [31,33–38].

III. RESULTS

A. Phase shifts

Table I presents a convergence study of the total energy E in Eq. (4), the confining parameter G in Eq. (7), and the S -wave phase shift δ_k at $k = 0.1$ and $R_0 = 17$ as the size of the basis set N increases progressively. Here the proton mass is taken to be 1836.152 673 89 [40], and the ground-state energy of H₂ is $E_{\text{H}_2} = -1.164 025 030 88$ [41], yielding the many-body eigenenergy $E = E_{\text{Ps}} + E_{\text{H}_2} + k^2/(2\mu) = -1.411 523 670$ at $k = 0.1$. As can be seen, E , G , and δ_k are smoothly converged to the ninth, fourth, and third significant digits, respectively. Table II presents a convergence study of λ in Eq. (10) and δ_k as the confining radius R_0 increases, where $k = 0.1$ and $N = 4400$. We can see that both

TABLE I. Convergence of the total energy E , the confining parameter G , and the S -wave phase shift δ_k (in radians) at $k = 0.1$ and $R_0 = 17$ as the size of the basis set N increases.

N	E	G	δ_k
4000	-1.411 523 665	$2.224 62 \times 10^{-5}$	-0.182 23
4200	-1.411 523 666	$2.225 01 \times 10^{-5}$	-0.182 15
4400	-1.411 523 667	$2.225 47 \times 10^{-5}$	-0.182 06
4600	-1.411 523 668	$2.225 67 \times 10^{-5}$	-0.182 02

TABLE II. Convergence of λ and the S -wave phase shift δ_k (in radians) at $k = 0.1$ and $N = 4400$ as the confining radius R_0 increases. The confining parameter G in Eq. (7) is also listed.

R_0	G	λ	δ_k
15	$1.489 021 6 \times 10^{-5}$	0.059 30	-0.181 7
16	$1.806 999 1 \times 10^{-5}$	0.059 36	-0.181 9
17	$2.225 472 6 \times 10^{-5}$	0.059 42	-0.182 1
18	$2.786 562 6 \times 10^{-5}$	0.059 48	-0.182 2

λ and δ_k converge smoothly to the third significant digit. We thus fix $N = 4400$ and $R_0 = 17$ in all the other calculations. Due to the limited ECG basis size and limited R_0 size, the uncertainty of the bound-state calculations for the confined Ps-H₂ system is the main source of phase-shift uncertainty.

Table III lists a comparison of the S -wave phase shifts obtained using the present non-BO CVM, the CVM with the fixed-nucleus approximation (FNA) [31], and the pseudopotential (PP) methods with and without the van der Waals potential (vdWP) [21]. For the case of incident momentum greater than $k = 0.14$ (i.e., the corresponding energy is 0.13 eV), such as $k = 0.16$, we cannot obtain a stable and converged numerical result when optimizing the lowest eigenenergy of the confined system. Although the optimization of higher eigenenergy levels may resolve this issue, it would take much longer to reach the same accuracy as for $k \leq 0.14$. Note that the phase shifts of the PP method are extracted directly from Fig. 5 of Ref. [21]. For $k < 0.1$ the extraction of the phase shift is difficult, and thus, the results are not shown. Comparing the non-BO CVM and FNA-CVM values, we can see that the phase shift increases when the FNA is removed and that for $\delta_{0.1}$ the percentage difference is 1.4%. In our previous work on Ps-H scattering [38], we found that the percentage difference in the phase shift between the infinite-nuclear-mass and finite-nuclear-mass cases is 0.1% for singlet scattering and 0.01% for triplet scattering, respec-

TABLE III. Comparison of S -wave phase shifts (in radians) among the present non-BO confined variational method (non-BO CVM), the CVM with the fixed-nucleus approximation (FNA-CVM), the pseudopotential (PP) method, and the PP with the van der Waals potential (vdWP-PP).

Method	k	δ_k
Non-BO CVM	0.04	-0.0780
	0.06	-0.1113
	0.08	-0.1455
	0.10	-0.1821
	0.12	-0.2202
FNA-CVM [31]	0.14	-0.2581
	0.099 993	-0.1846
PP [21]	0.10	-0.2054
	0.12	-0.2455
	0.14	-0.2862
vdWP-PP [21]	0.10	-0.0761
	0.12	-0.0947
	0.14	-0.1141

TABLE IV. S -wave phase shifts (in radians) calculated using the model potential in Eq. (10) (first entry) and in Eq. (12) (second entry), subject to the same confining potential.

k	G	λ	δ_0
0.06	$9.885\,991\,2 \times 10^{-7}$	0.056\,735\,317\,5	-0.111\,336
		0.042\,360\,940\,6	-0.111\,334
0.10	$2.225\,472\,6 \times 10^{-5}$	0.059\,419\,332\,4	-0.182\,056
		0.044\,7948\,222	-0.182\,056
0.14	$4.724\,490\,9 \times 10^{-4}$	0.065\,817\,067\,3	-0.258\,055
		0.050\,824\,126\,7	-0.258\,065

tively. The larger percentage difference between the non-BO CVM and FNA-CVM phase shifts for Ps-H₂ scattering may originate from the complicated interaction caused by the nuclear motion. Finally, it is unexpected that the PP values are closer to our non-BO CVM values than the vdWP-PP ones are.

To better understand the role of the van der Waals potential, the model potential without the van der Waals part

$$\mathcal{V}_m(\rho) = \lambda e^{-0.5\rho} \quad (12)$$

was also tested in our calculation, and the results are shown in Table IV. We can clearly see that V_m and \mathcal{V}_m result in the same phase shifts when they are subject to the same confining energy E' and confining potential v_{cp} . This means that although the vdWP correctly describes the long-range interaction between Ps and H₂, the effect of the vdWP term in Eq. (10) can almost completely be recovered by tuning λ in Eq. (12). In fact, the effect of vdWP is automatically included in the calculation of the confined many-body bound-state problem Eq. (4).

Replacing the potential $\lambda e^{-\alpha\rho}$ in Eqs. (10) and (12) with the typical Ps-H₂ pseudopotential $\lambda_t e^{-\alpha_t\rho}/\rho^3$ with $\alpha_t = 0.2439$ [21] and solving Eq. (9), we obtain the same values of phase shifts as those of the non-BO CVM listed in Table III. Table V presents the CVM values of λ_t determined using Eq. (9) for the cases with and without the vdWP included. They are all smaller than the value of $\lambda_t = 5.919$ adopted in the vdWP-PP and PP calculations [21]. Once again, our calculations have shown that the CVM does not depend on the concrete forms of model potentials, provided their short-range potentials vanish at R_0 .

B. Scattering length and cross section

The S -wave scattering length is obtained by fitting the calculated phase shifts to the variants of well-known effective

TABLE V. CVM values of λ_t for case 1 with the vdWP included and case 2 without the vdWP for different incident momenta k . In atomic units.

	k					
	0.04	0.06	0.08	0.1	0.12	0.14
Case 1	1.512 9	1.400 8	1.368 9	1.389 5	1.430 7	1.467 3
Case 2	1.0414	0.944 9	0.921 3	0.945 2	0.988 1	1.027 6

TABLE VI. S -wave scattering lengths obtained with the present confined variational method (non-BO CVM), the CVM with the fixed-nucleus approximation (FNA-CVM), the stabilization method with the fixed-nucleus approximation (FNA-SM), the pseudopotential (PP) method, and the PP with the van der Waals potential (vdWP-PP). In atomic units.

Method	Scattering length
Non-BO CVM, Eq. (13)	2.08
Non-BO CVM, Eq. (14)	1.97
FNA-CVM, Eq. (14) [31]	2.02
FNA-SM, Eq. (13) [31]	1.78
PP [21]	2.06
vdWP-PP [21]	0.64
Experiment [24]	2.1 ± 0.2

range theory,

$$\cot(\delta_k) = -\frac{1}{A_0 k} + \frac{1}{2}r_0 k + Bk^2, \quad (13)$$

where A_0 is the S -wave scattering length, r_0 is the effective range, and B is an additional fitting parameter. Taking into account the long-range van der Waals potential $-C_6/\rho^6$, we should use the modified effective range formula [42]

$$\cot(\delta_k) = -\frac{1}{A_0 k} + \frac{r_0 k}{2} - \frac{4\pi C_6 k^2}{15A_0^2} - \frac{16C_6 k^3 \ln(k)}{15A_0}. \quad (14)$$

Table VI presents a comparison of the S -wave scattering lengths obtained with the present non-BO CVM, the FNA-CVM [31], the stabilization method (FNA-SM) [31], the PP, the vdWP-PP [21], and the angular correlation of annihilation radiation (ACAR) experiment [24]. The ACAR value is estimated from the average momentum-transfer cross section for scattering energy below 0.3 eV. To extract a more accurate scattering length, phase shifts at lower k are more suitable for the fitting. Thus, phase shifts at $k = 0.04$ – 0.1 were used in the present work. The non-BO CVM value determined with Eq. (14) is 5.6% smaller than that determined with Eq. (13), indicating that the long-range potential has a significant effect on the scattering length. Comparing the non-BO CVM and FNA-CVM values at the internuclear distance $R_{pp} = 1.45a_0$, we can see that the FNA effect increases the scattering length by 2.5%. The FNA-SM value, which is extracted from the phase shifts at $k = 0$ – 0.5 with Eq. (13), is 17% smaller than the non-BO CVM value obtained with Eq. (13). The PP value is closer to our value than the vdWP-PP one is, similar to the case of phase shifts. It is noted that the scattering lengths of the non-BO CVM, FNA-CVM, and PP methods fall into the error bars of the experimental value.

Figure 1 shows a comparison of theoretical and experimental cross sections for $k < 0.2$. We denote σ_m as the momentum-transfer cross section and σ_t as the total cross section. At low energy, σ_m and σ_t can be calculated by using

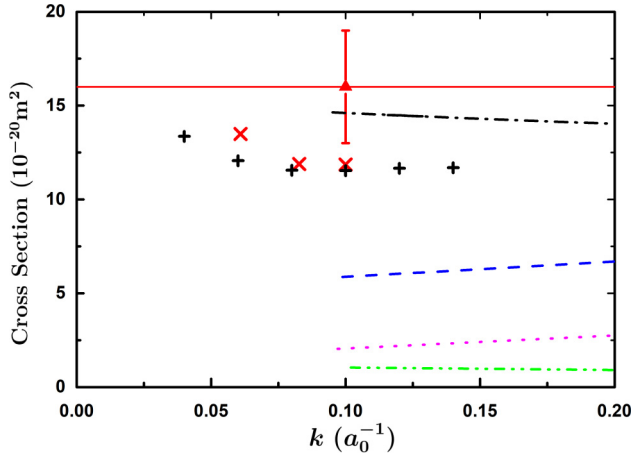


FIG. 1. Comparison of the cross sections for $k < 0.20$. Theory: non-BO CVM (black pluses); Zhang *et al.*, FNA-CVM (red crosses) [31]; Wilde and Fabrikant, PP (dash-dotted black line) and vdWP-PP (dotted magenta line) [21]; Wilde and Fabrikant, FEG (dashed blue line) and OPP-FEG (dash-double-dotted green line) [32]. Experiment: Satio *et al.*, ACAR (red triangle) [24].

the partial-wave expansion:

$$\begin{aligned}\sigma_m &= \frac{4\pi}{k^2} \sum_{l=0}^{\infty} (l+1) \sin^2(\delta_k^{l+1} - \delta_k^l), \\ \sigma_t &= \frac{4\pi}{k^2} \sum_{l=0}^{\infty} (2l+1) \sin^2 \delta_k^l,\end{aligned}\quad (15)$$

where δ_k^l is the phase shift of the l th partial wave at momentum k . At $k \leq 0.14$, the S -wave scattering is dominant in σ_m and σ_t . For example, $\delta_{0.14}^1$ of PP (extracted directly from Fig. 5 of Ref. [21]) is -0.00996 rad, which is much smaller than $\delta_{0.14}^0$ and can thus be neglected. Therefore, σ_m and σ_t of the non-BO CVM are calculated using only the S -wave phase shifts. We can see that the elastic-scattering cross sections of the non-BO CVM decrease smoothly as k increases. Overall, the cross sections obtained with non-BO CVM, FNA-CVM, and PP calculations agree well with the ACAR experimental value of Saito *et al.* [24]. The theoretical results of vdWP-PP, the free-electron-gas (FEG) approximation, and the FEG with an orthogonalizing pseudopotential (OPP-FEG) [32] are much lower than the ACAR value but are close to the experimental value of $(3.34 \pm 0.7) \times 10^{-16} \text{cm}^2$ from the Doppler broadening spectroscopy (DBS) method carried out by Skalsey *et al.* [26]. Similar to the Ps-He scattering [37], our Ps-H₂ low-energy CVM cross sections may imply that the DBS σ_m values are questionable.

C. Distortion effects

The H₂ molecule and Ps will be distorted when they get close to each other. In the previous study of Biswas and Adhikari [29,30], three Ps pseudostates Ps($1s$), Ps($2s$), and Ps($2p$) were included with the internuclear distance $R_{pp} = 1.4a_0$. In the calculation of Zhang *et al.* [31], the distortion of Ps was well described by using the ECG basis functions with $R_{pp} = 1.45a_0$. Using the Hartree-Fock method, Wilde and

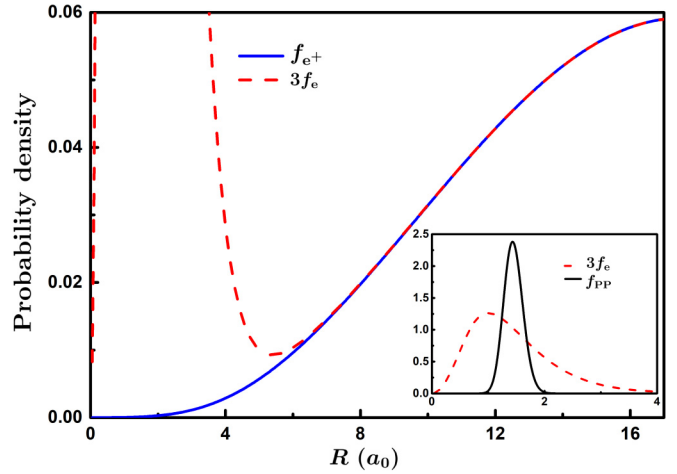


FIG. 2. Probability density distributions of the distance between the two protons f_{pp} , between the electron and the center of the two protons f_e , and between the positron and the center of the two protons f_{e^+} .

Fabrikant [32] calculated the charge densities, which could be converted to exchange and correlation potentials.

To quantitatively study the distortion effects, we define three distortion distances R_{Ps}^d , $R_{H_2}^d$, and $R_{Ps-H_2}^d$, where R_{Ps}^d and $R_{H_2}^d$ are measures of the distance between Ps and H₂ when the distortion of Ps or H₂ can be ignored, respectively, and $R_{Ps-H_2}^d$ is a measure of this distance when the distortion of both Ps and H₂ can be ignored. When the distance between Ps and H₂ is larger than $R_{Ps-H_2}^d$, the long-range van der Waals potential $-C_6/\rho^6$ is dominant. As the polarizability of Ps ($\alpha = 36a_0^3$) is larger than that of H₂ ($\alpha = 5.4a_0^3$), the distortion of Ps dominates over that of H₂, implying $R_{Ps-H_2}^d = \max(R_{Ps}^d, R_{H_2}^d) = R_{Ps}^d$.

The probability density distribution of the electron, relative to the center of the two nuclei, is

$$f_e^i(R) = \int d\Omega_{\mathbf{R}} \langle \Psi | \delta(\mathbf{x}_i - \mathbf{x}_1/2 - \mathbf{R}) | \Psi \rangle R^2, \quad (16)$$

where $i = 2, 3, 4$. Since the three electrons are identical, we have $f_e^2(R) = f_e^3(R) = f_e^4(R) \equiv f_e(R)$. Similarly, the probability density distribution of the positron is

$$f_{e^+}(R) = \int d\Omega_{\mathbf{R}} \langle \Psi | \delta(\mathbf{x}_5 - \mathbf{x}_1/2 - \mathbf{R}) | \Psi \rangle R^2. \quad (17)$$

Because of the electric neutrality requirement of Ps at $R \geq R_{Ps}^d$, the distortion distance R_{Ps}^d can be obtained according to

$$f_{e^+}(R) = 3f_e(R), \quad R \geq R_{Ps}^d. \quad (18)$$

The probability density distributions at $k = 0.1$ are plotted in Fig. 2. For $f_e(R)$, high peak exists near $R = 1.0$, while the density of the scattering electron is lower for $R > 8.0$. For $f_{e^+}(R)$, there is no peak for $R < 4.0$ due to the repulsive interaction between the positron and the two protons. Compared to $f_{e^+}(R)$ of the Ps-H singlet scattering in our previous work [38], $f_{e^+}(R)$ of the Ps-H has a low peak at $k = 0.1$ for $R < 4.0$. We can see that the probability density distributions of the electron and positron become similar when $R \geq 6.0$. In this work, R_{Ps}^d is determined according to

$|1 - 3f_e(R_{\text{Ps}}^d)/f_{e^+}(R_{\text{Ps}}^d)| \leq 1\%$. Using this criterion, we obtain $R_{\text{Ps}}^d = 7.8, 7.25, \text{ and } 6.95$ at $k = 0.06, 0.1, \text{ and } 0.14$, respectively, which indicates that R_{Ps}^d decreases as k increases. Without the fixed-nucleus approximation, we can study the distortion of the H_2 molecule. The probability density distribution of the distance between the two protons at $k = 0.1$, which is calculated by $f_{\text{pp}}(R) = \int d\Omega_R \langle \Psi | \delta(\mathbf{x}_1 - \mathbf{R}) | \Psi \rangle R^2$, is also plotted in Fig. 2. We can see that the most probable internuclear distance is $R_{\text{pp}}^{\text{mp}} = 1.433$, which is between the values used by Biswas and Adhikari [29,30] and by Zhang *et al.* [31]. Actually, $R_{\text{pp}}^{\text{mp}}$ for $k = 0.06$ and 0.14 is also 1.433 with $f_{\text{pp}}(1.433)$ equal to 2.3814 and 2.3810 , respectively. As expected, such low-energy elastic Ps collisions barely affect the motion of two protons in the target H_2 .

IV. SUMMARY

By treating the motion of nuclei and leptons on an equal footing, together with ECG variational functions, the non-BO CVM has been applied to calculate the S -wave phase shifts, scattering length, and cross sections for the low-energy elastic Ps- H_2 scattering. Compared with the previous FNA-CVM, the non-BO CVM phase shift at $k = 0.1$ differs from the

FNA-CVM phase shift by about 1.4%. Unexpectedly, the non-BO CVM phase shifts are closer to those calculated with the PP method than to those calculated with the vdWP-PP method. Overall, the non-BO CVM cross sections agree well with the FNA-CVM and PP theoretical calculations and with the ACAR experimental value of Saito *et al.* [24]. The results from the non-BO CVM may imply that the DBS σ_m cross sections are questionable. The Ps distortion distances R_{Ps}^d are $7.8, 7.25, \text{ and } 6.95$ for $k = 0.06, 0.1, \text{ and } 0.14$, respectively, which indicates that R_{Ps}^d decreases as k increases.

ACKNOWLEDGMENTS

This work was supported by the National Natural Science Foundation of China under Grants No. 11704399, No. 11934014, and No. 12174399, by the Strategic Priority Research Program of the Chinese Academy of Sciences under Grant No. XDB21030300, and by the National Key Research and Development Program of China under Grant No. 2017YFA0304402. M.-S.W. was supported by the Initial Scientific Research Fund of Hainan University under Grant No. KYQD(ZR)-21158. Z.-C.Y. was supported by NSERC of Canada.

-
- [1] S. G. Karshenboim, *Phys. Rep.* **422**, 1 (2005).
 [2] T. Yamazaki, A. Miyazaki, T. Suehara, T. Namba, S. Asai, T. Kobayashi, H. Saito, I. Ogawa, T. Idehara, and S. Sabchevski, *Phys. Rev. Lett.* **108**, 253401 (2012).
 [3] G. S. Adkins, M. Kim, C. Parsons, and R. N. Fell, *Phys. Rev. Lett.* **115**, 233401 (2015).
 [4] C. Frugieule, J. Pérez-Ríos, and C. Peset, *Phys. Rev. D* **100**, 015010 (2019).
 [5] L. Gurung, T. J. Babij, S. D. Hogan, and D. B. Cassidy, *Phys. Rev. Lett.* **125**, 073002 (2020).
 [6] A. J. Garner, G. Laricchia, and A. Ozen, *J. Phys. B* **29**, 5961 (1996).
 [7] A. Garner, A. Ozen, and G. Laricchia, *Nucl. Instrum. Methods Phys. Res., Sect. B* **143**, 155 (1998).
 [8] A. J. Garner, A. Ozen, and G. Laricchia, *J. Phys. B* **33**, 1149 (2000).
 [9] S. J. Brawley, S. E. Fayer, M. Shipman, and G. Laricchia, *Phys. Rev. Lett.* **115**, 223201 (2015).
 [10] C. M. Surko, M. Leventhal, and A. Passner, *Phys. Rev. Lett.* **62**, 901 (1989).
 [11] A. S. Kadyrov, I. Bray, M. Charlton, and I. I. Fabrikant, *Nat. Commun.* **8**, 1544 (2017).
 [12] M. Charlton, H. B. Ambalampitiya, I. I. Fabrikant, D. V. Fursa, A. S. Kadyrov, and I. Bray, *Phys. Rev. A* **104**, L060803 (2021).
 [13] S. J. Brawley, A. I. Williams, M. Shipman, and G. Laricchia, *Phys. Rev. Lett.* **105**, 263401 (2010).
 [14] S. J. Brawley, S. Armitage, J. Beale, D. E. Leslie, A. I. Williams, and G. Laricchia, *Science* **330**, 789 (2010).
 [15] G. F. Gribakin, J. A. Young, and C. M. Surko, *Rev. Mod. Phys.* **82**, 2557 (2010).
 [16] D. G. Green, A. R. Swann, and G. F. Gribakin, *Phys. Rev. Lett.* **120**, 183402 (2018).
 [17] D. Woods, S. J. Ward, and P. Van Reeth, *Phys. Rev. A* **92**, 022713 (2015).
 [18] J. E. Blackwood, M. T. McAlinden, and H. R. J. Walters, *Phys. Rev. A* **65**, 032517 (2002).
 [19] M. W. J. Bromley and J. Mitroy, *Phys. Rev. A* **66**, 062504 (2002).
 [20] J. Mitroy and M. W. J. Bromley, *Phys. Rev. A* **68**, 035201 (2003).
 [21] R. S. Wilde and I. I. Fabrikant, *Phys. Rev. A* **92**, 032708 (2015).
 [22] I. I. Fabrikant and G. F. Gribakin, *Phys. Rev. Lett.* **112**, 243201 (2014).
 [23] Y. Nagashima, M. Kakimoto, T. Hyodo, K. Fujiwara, A. Ichimura, T. Chang, J. Deng, T. Akahane, T. Chiba, K. Suzuki, B. T. A. McKee, and A. T. Stewart, *Phys. Rev. A* **52**, 258 (1995).
 [24] F. Saito, Y. Nagashima, and T. Hyodo, *J. Phys. B* **36**, 4191 (2003).
 [25] M. Skalsey, J. J. Engbrecht, R. K. Bithell, R. S. Vallery, and D. W. Gidley, *Phys. Rev. Lett.* **80**, 3727 (1998).
 [26] M. Skalsey, J. J. Engbrecht, C. M. Nakamura, R. S. Vallery, and D. W. Gidley, *Phys. Rev. A* **67**, 022504 (2003).
 [27] M. Comi, G. Prosperi, and A. Zecca, *Phys. Lett. A* **93**, 289 (1983).
 [28] P. Biswas and A. Ghosh, *Phys. Lett. A* **223**, 173 (1996).
 [29] P. K. Biswas and S. K. Adhikari, *J. Phys. B* **31**, L737 (1998).
 [30] P. K. Biswas and S. K. Adhikari, *J. Phys. B* **33**, 1575 (2000).
 [31] J.-Y. Zhang, M.-S. Wu, Y. Qian, X. Gao, Y.-J. Yang, K. Varga, Z.-C. Yan, and U. Schwingenschlögl, *Phys. Rev. A* **100**, 032701 (2019).
 [32] R. S. Wilde and I. I. Fabrikant, *J. Phys.: Conf. Ser.* **1412**, 052011 (2020).

- [33] J. Mitroy, J. Y. Zhang, and K. Varga, *Phys. Rev. Lett.* **101**, 123201 (2008).
- [34] J. Y. Zhang, J. Mitroy, and K. Varga, *Phys. Rev. A* **78**, 042705 (2008).
- [35] J.-Y. Zhang, Z.-C. Yan, and U. Schwingenschläžšgl, *Europhys. Lett.* **99**, 43001 (2012).
- [36] J.-Y. Wan, M.-S. Wu, J.-Y. Zhang, and Z.-C. Yan, *Phys. Rev. A* **103**, 042814 (2021).
- [37] M.-S. Wu, J.-Y. Zhang, X. Gao, Y. Qian, H.-H. Xie, K. Varga, Z.-C. Yan, and U. Schwingenschlöggl, *Phys. Rev. A* **101**, 042705 (2020).
- [38] M.-S. Wu, J.-Y. Zhang, Y. Qian, K. Varga, U. Schwingenschlöggl, and Z.-C. Yan, *Phys. Rev. A* **103**, 022817 (2021).
- [39] J. Mitroy, S. Bubin, W. Horiuchi, Y. Suzuki, L. Adamowicz, W. Cencek, K. Szalewicz, J. Komasa, D. Blume, and K. Varga, *Rev. Mod. Phys.* **85**, 693 (2013).
- [40] P. J. Mohr, D. B. Newell, and B. N. Taylor, *Rev. Mod. Phys.* **88**, 035009 (2016).
- [41] L. M. Wang and Z.-C. Yan, *Phys. Rev. A* **97**, 060501(R) (2018).
- [42] G. W. F. Drake, *Springer Handbook of Atomic, Molecular, and Optical Physics* (Springer, New York, 2006), p. 668.